Experimental study on the use of granulometric speciation for the radiometric dating of recent sediments

Juan Mantero[a], José M. Abril Hernández[b,*], Rafael García-Tenorio[a,c], Emmanuel Klubi[d], Elvis Nyarko[d,e]

[a] Departamento de Física Aplicada II, Universidad de Sevilla. ETSA, Seville, Spain
[b] Departamento de Física Aplicada I. Universidad de Sevilla. ETSIA, Seville, Spain
[c] Centro Nacional de Aceleradores (Univ. Sevilla- J. Andalucía-CSIC), Seville, Spain
[d] Department of Marine and Fisheries Sciences, University of Ghana, Legon, Ghana
[e] Vice Chancellor of the Regional Maritime University, Accra, Ghana

Keywords:

Radiometric dating

Granulometric speciation

Gamma spectrometry

Detection limit

Normalized activities

A B S T R A C T

Theoretical and experimental studies have shown that activity concentrations of fallout radionuclides (such as ^{137}Cs and excess ^{210}Pb) decrease with particles size in aqueous suspensions. This paper is aimed at reviewing the theoretical fundamentals for granulometric speciation of radionuclides, and at exploring its practical use in the analytical context of gamma spectrometry for the radiometric dating of recent sediments, with view to: i) im-proving the detection of ^{137}Cs (since its use as independent chronostratigraphic mark is challenging in the southern hemisphere because its low fallout rate), ii) supporting refined CIC models and normalization tech-niques in ^{210}Pb-based radiogeochronologies. The work uses surface sediments sampled from the Tinto Estuary (SW Spain), affected by mining and phosphate-fertilizer industries, and from the Ankobra Estuary (Ghana), affected by intensive artisanal gold-mining. Granulometric classes have been separated by a sieving column with decreasing mesh sizes and the obtained cumulative percentage of mass mathematically described by a Rosin-Rammler particle-size distribution. The target radionuclides for gamma spectrometry were ^{210}Pb, ^{226}Ra and^{137}Cs, complemented with ^{40}K, ^{234}Th and ^{228}Ra. Results revealed that, far from ideal experiments, under actual environmental conditions the increase in activity concentrations with decreasing particle sizes is too moderate, and in general they are affected by larger counting uncertainties due to the small available amount of mass. Indeed, there was no correlation between grain-size and ^{137}Cs concentrations (p = 0.25), and similarly for excess ^{210}Pb (p = 0.53). No effect of the organic matter content was observed in ^{137}Cs (p = 0.58) and excess ^{210}Pb (p = 0.85) concentrations. Present results pose some concerns to the general use of granulometric speciation in the context of gamma spectrometry for supporting the radiometric dating of recent sediments. A detailed discussion on the use of normalization methods is also presented.

1. Introduction

Radiometric chronologies for recent sediment cores can provide reliable estimates of sediment accumulation rates and deposition processes, which are the keys for inferring past environmental conditions and for decoding anthropogenic pollution records (Carroll and Lerche, 2003). For recent sediments (< 100–150 y) the most common dating technique is based in the use of fallout ^{210}Pb, a natural radionuclide (Robbins, 1978; Appleby, 2001; Mabit et al., 2014).

The physical fundamentals for the mass-conservation of a particle-bound radioactive tracer, such as unsupported ^{210}Pb, in porous and accreting sediments are relatively well understood (see the revisited diagenetic equations in Abril, 2003). Nevertheless, unsupported ^{210}Pb *versus* mass depth profiles can be the result of many different sedimentological settings, involving varying boundary conditions (fluxes of matter and radionuclides at the sediment water interface) and post-depositional processes such as diffusion or mixing, which results in different chronologies (Abril, 2015). Because of this, some bomb-fallout radionuclides such as ^{137}Cs, $^{239+240}$Pu and ^{241}Am, are often used for providing independent chronostratigraphic marks (Kim et al., 1997; Alonso-Hernández et al., 2006; Abril et al., 2018) to help in the selection of the most appropriate ^{210}Pb chronology.

The above radiometric dating tools ultimately rely on the ability of solid particles in the sediment for irreversibly binding some

* Corresponding author. Departamento de Física Aplicada I, ETSIA, Universidad de Sevilla, Carretera de Utrera km 1, D.P., 41013, Sevilla, Spain.
E-mail address: jmabril@us.es (J.M. Abril Hernández).

radionuclides and trace elements. It is well known from theoretical studies (Abril, 1998a, 1998b) and laboratory experiments with radioactive tracers (El Mrabet et al., 2001; Barros and Abril, 2005) that the uptake by suspended particulate matter in aqueous suspension is a surface-mediated phenomenon, and, consequently, that the activity concentrations increase with the specific surface area of particles. A quite straightforward and well-known consequence is that the distribution coefficients (k_d, the ratio between activity concentrations in solids and water) for these radionuclides (adsorbed at the particles surface, but absent from their inner matrices) decrease as the particles size increase (Abril and Fraga, 1996).

The simplest ^{210}Pb-based model is the one assuming constant flux and constant sedimentation (CF-CS), along with ideal deposition and non-postdepositonal redistribution. Under these conditions the unsupported or excess ^{210}Pb (^{210}Pb$_{exc}$) *versus* mass depth profile is an exponential function. The best mathematical fit of this function to the dataset allows for estimating the mass sedimentation rate, and then the chronology (see Sánchez-Cabeza and Ruíz-Fernández, 2012). But, this mentioned fit may be poor in non-monotonic and noisy ^{210}Pb$_{exc}$ profiles, which often appear when the granulometry of the mineral solids in the sediment largely varies with depth.

Some authors assume that the sand content of a sediment slice is virtually free of ^{210}Pb$_{exc}$ (e.g., Sanders et al., 2012), and then they report and use mud-normalized concentrations for applying the CF-CS model (Ruiz-Fernández et al., 2009; Sanders et al., 2012). Pedersen et al. (2007) applied a more complex normalization formula for ^{210}Pb$_{exc}$ and ^{137}Cs, involving the contribution of both, Loss-On-Ignition (LOI) and the amount of minerogenic material smaller than 30 μm. It is worth noting that other normalization methods have been proposed for improving the performance of the CF-CS but involving other parameters instead of the granulometry, such as LOI (Kim et al., 1997; Van Eaton et al., 2010), Al_2O_3 (Cundy and Croudace, 1996) or Al (Álvarez-Iglesias et al., 2007). Clay-normalized ^{210}Pb activity concentrations have been used for establishing geochronologies of flood events in large tropical river systems (Aalto and Nittrouer, 2012). Recently, Sun et al. (2018) reported results on extensive study of granulometry and ^{210}Pb$_{exc}$ activity concentrations involving 11 cores sampled in the coastal area of the Yangtze River Estuary. They found a strong positive correlation ($r = 0.829$) between the clay component (< 4 μm) and ^{210}Pb$_{exc}$ in all the sediment cores. They then used clay-normalized ^{120}Pb$_{exc}$ profiles for the radiometric dating of the cores.

The above normalization procedures use the information on particles size distributions, but they do not involve the direct measurement of ^{210}Pb in the physically-separated grain-size classes (hereafter referred as granulometric speciation). Granulometric speciation has been applied previously for identifying anthropogenic inputs of some NORM-radionuclides in estuarine sediments (Laissaoui and Abril, 1999). The key idea was identifying, in the small-grain-size fraction of the sediments, the singular fingerprint of surface-bound radionuclides, consisting in higher activity concentrations. A similar approach could be intended for improving the detection of the bomb-fallout radionuclides in sediment cores from the southern hemisphere. Effectively, it is well-known that the low fallout rate at these geographical latitudes causes a serious limitation for using these radionuclides as independent chronostratigraphic markers for supporting and/or validating the ^{210}Pb-based geochronologies (e.g., Hancock et al., 2011; Klubi et al., 2017). Thus, measuring activity concentrations of these bomb-fallout radionuclides along the core in a homogeneously defined grain-size class could provide a sound method for identifying the chronostratigraphic mark associated to the 1963 fallout peak. Moreover, measuring ^{210}Pb$_{exc}$ in the above homogeneously defined grain-size class is consistent with the CIC-model assumptions (constancy of the initial activity concentration –now understood for a target grain-size class), and it could improve its performance by reducing the noise (and the age reversals) resulting from the contribution of coarse particles in sediments with varying granulometries.

Although the fundamentals of radionuclide uptake by suspended particulate matter in spiked aqueous solutions are clear, the situation is more complex within the saturated porous media of sediments, even under ideal experimental conditions. Effectively, it has been also shown that the direct uptake of dissolved radionuclides in the water-column by surficial sediments is governed by physical diffusion and by the fraction of the particles surface which is actually accessible to the pore-water (Barros et al., 2004). On the other hand, natural conditions may be quite different from the well-controlled laboratory experiments. Thus, in natural sediments, radionuclide activity concentrations in different grains are expected to be the composite result of a large diversity of histories of varying contact-times of particle surfaces within aqueous solutions with varying activity concentrations. It is also worth noting that the available mass of the selected small grain size fraction in a sediment slice may limit the potential improvement of minimum detectable activities (MDA) for bomb-fallout radionuclides by granulometric speciation.

This paper is aimed at reviewing the theoretical fundamentals for granulometric speciation and for exploring its practical use in the analytical context of gamma spectrometry for improving the detection of ^{137}Cs and for supporting refinements in the application of the CIC model and in the normalization techniques for others ^{210}Pb-based models. In this work are used surface sediments sampled from the Tinto Estuary (SW Spain) and the Ankobra Estuary (Ghana). The first being historically affected by mining activities and releases from chemical industries, including phosphate fertilizers (Guerrero-Márquez et al., 2017), and the second nowadays seriously affected by artisanal gold-mining activities (Klubi et al., 2018).

2. Materials and methods

2.1. Theoretical considerations on granulometric speciation

The goal of this section is deriving a quantitative estimate of the factor by which the net number of counts in a photopeak can be higher in a selected grain-size subsample with respect to the bulk sediment sample, when gamma-ray spectrometry is performed.

After sieving a sediment sample, the cumulative percentages of mass (given as a dimensionless fraction) at each diameter level, $y(x) - x$ being the diameter, can be fitted by a Rosin-Rammler (R-R) particle-size distribution (Vesilind, 1980):

$$y(x) = 1 - e^{-\left(\frac{x}{x_0}\right)^n}, \tag{1}$$

where n and x_0 are fitted parameters. Its first derivative provides the frequency distribution of particles with diameter x, $C(x) = dy/dx$, allowing then the estimation of mean and modal values.

Theoretical and experimental studies with spiked aqueous suspensions show that the uptake of dissolved radionuclides is governed by the surface area of particles. Assuming that the activity of a given fallout radionuclide bound to the sediment particles of diameter x is proportional to their free surface, $S(x)$, the activity concentration, $A(x)$, can be estimated as

$$A(x) = \frac{kS(x)}{\rho V(x)}, \tag{2}$$

where $V(x)$ is the volume of particles of diameter x, ρ is their density, and k is the scaling factor. Under the simplifying assumption of spherical-shaped particles,

$$A(x) = \frac{6k}{\rho x}. \tag{3}$$

The mean activity concentration of the sediment subsample with diameters ranging from zero up to a certain diameter x_c, $A_m(x_c)$, is then

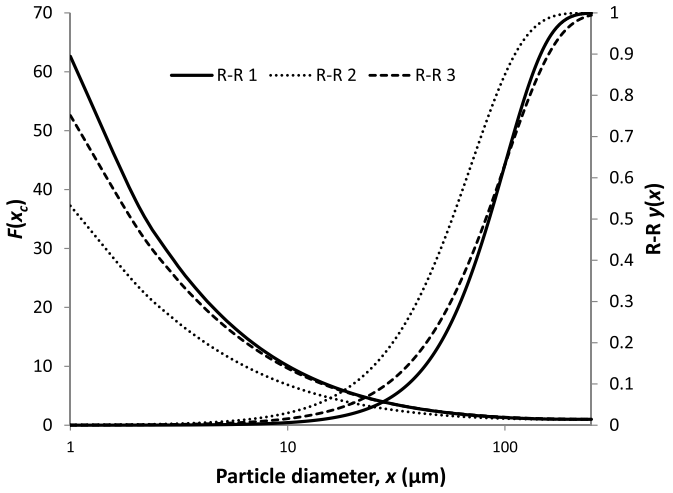

Fig. 1. Factor of merit $F(x_c)$ estimated as a function of the cutting diameter (by using Eqs. (1)–(5)) for various Rosin-Rammler particle-size distributions $y(x)$ (Eq. (1)) with parameters values (x_0, n) of (100, 2.2), (70, 1.8) and (100, 1.8) for distributions R-R 1, R-R 2 and R-R 3, respectively (x_0 given in μm). The main vertical axis, with decreasing lines, is for $F(x_c)$, while the corresponding $y(x)$ distribution, with increasing lines, are plotted with the secondary axis.

$$A_m(x_c) = \frac{1}{y(x_c)} \int_0^{x_c} A(x)C(x)dx; \tag{4}$$

and the activity concentration for the bulk sediment sample, A_b, is given by Eq. (4) for $x_c \to \infty$. Here we are interested in the ratio

$$F(x_c) = A_m(x_c)/\, A_b, \tag{5}$$

because it is the factor by which the activity concentration of a subsample of sediment particles with diameter lower than x_c is higher than the activity concentration measured in the bulk sample (x_c will be referred as cutting diameter hereafter).

Fig. 1 shows a plot of $F(x_c)$ for various R-R particle-size distributions. It is worth noting that the parameters k and ρ cancel out in the estimation of $F(x_c)$ when both are assumed to be constant. The factor $F(x_c)$ could take values over 10 for cutting diameters of few μm, and it increases with parameters x_0 and n in the R-R distribution (Eq. (1)).

For analytical methods requiring small amounts of sample (such as alpha spectrometry) $F(x_c)$ gives a primary figure of merit (a quantity used to characterize the performance of a method, relative to its alternatives). Nevertheless, and as also shown in Fig. 1, as higher is $F(x_c)$, lower is the fraction in mass of the sample $y(x_c)$. For gamma spectrometry, the net number of counts in a photopeak, N_S, depends on the activity concentration of the sample, A, its mass, m, the intensity of the γ-emission, I, the efficiency, ε, and the counting time, t: . Thus, for the same counting time, the factor F_N by which N_S increases when measuring the subsample with particles size below x_c with respect to the bulk sample (in different sample-adapted geometries) is

$$F_N = \frac{A_m(x_c)\, m(x_c)\varepsilon(x_c)}{A_b m_b \varepsilon_b} = F(x_c)\frac{m(x_c)\varepsilon(x_c)}{m_b \varepsilon_b} \tag{6}$$

Although $F(x_c)$ can take high values (Fig. 1) the goal for applications involving gamma spectrometry is maximizing F_N. The mass ratio can take the value of the unit as its upper limit, while its lower bound is the value of $y(x_c)$ –when the whole available masses are used. In practice, and in order to fit standardized counting geometries, m_b can be an aliquot of the total available mass of the sample, particularly for gamma spectrometry with well-type detectors. It is worth noting that for applications oriented to the granulometric speciation, coring devices with higher diameters could be selected. Additionally, the total available amount of bulk mass could be increased by using twin cores (when horizontal homogeneity can be assumed) or by thicker resolutions in the slicing of the core. This could provide a chance for increasing $m(x_c)$. Finally, small amount of samples could be accommodated in counting geometries with higher efficiencies than the geometry used for the bulk sample.

Self-absorption in the sample of low energy γ-emissions must be taken into account, particularly for ^{210}Pb. It may be different for the geometries selected for $m(x_c)$ and for m_b. The same applies for the Compton background. Consequently the potential of the granulometric speciation will be determined by comparing the MDA of subsamples with $x < x_c$ and the bulk sample, in their respective counting geometries.

The goal of the present work is testing with environmental sediment samples the use of the assumptions involved in the above estimation of $F(x_c)$, and the feasibility for achieving high F_N values with some real particle-size distributions and different counting geometries.

2.2. The studied estuaries

The Tinto River, with a length of about 100 km, is located in Southwestern Spain. Its sources are located in the Iberian Pyrite Bell where metal mining activities date back to prehistoric times. It drains to the Atlantic Ocean in the Huelva Estuary, where it joins the Odiel River. Since the 1960s large industrial complexes were located in the watershed of the estuary, including five plants devoted to the production of phosphoric acid and phosphate fertilizers. Although mining and phosphate fertilizers activities have recently ceased, the estuarine sediments still preserve the effect of enhanced concentrations of some natural radionuclides, particularly ^{226}Ra (Hierro et al., 2012; Guerrero-Marquez et al., 2017).

The Ankobra Estuary in Asanta, Nzema East district, Ghana, is the lower section of River Ankobra which takes its source from the North hills of Basindare, near Bibiani, and flows into the Atlantic Ocean at the south. The entrance of the estuary could be described as a sand ramp with abrupt increase in depth towards the freshwater end. The west coastline comprises sandy beaches with coconut plantations as defence structures. The estuary serves as fish landing site for the local community, and the riparian vegetation, mainly mangrove, provides niches for avifauna. Its geology is associated with alluvial gold deposits in basal rock underlying by meta-sedimentary and volcanic of the Biriamian and Tarkwaian systems. In this rural south-western portion of Ghana, the lack of industrial activities makes small-scale gold mining the main source of water contamination with potentially toxic elements (Klubi et al., 2018).

The sediment material from the Tinto Estuary was intended for assessing the fundamentals and use of the granulometric speciation with gamma spectrometry, whereas sediment samples from the Ankobra Estuary were mainly intended for assessing the use of this technique for improving the detection of ^{137}Cs in Equatorial Africa.

2.3. Sampling, sample preparation and granulometric analysis

Surface sediment samples were collected from each of the studied estuaries by using an Ekman grab. In the Tinto Estuary a single ~2 kg d.w. sample was collected on the 8th March 2017 at 37.2117°N, 6.9303°W below 2 m water depth. In the Ankobra Estuary 8 samples of ~0.15 kg d.w. were collected at the end of January 2017 covering a representative area (see Fig. 2). Precise positioning of each sampling location was marked using a Garmin Extrex GPS. Sampling depths ranged from 1 to 15 m.

Samples from the Ankobra were transferred into pre-labelled Ziplock™ bags, sealed and placed in a cooler and further stored frozen in the Marine and Fisheries' laboratory in the University of Ghana. These samples were latter thawed, dried at 50 °C using a Gallen Kamp Plus II oven to a constant weight, and re-packaged and transported to the laboratory of environmental radioactivity of the University of Seville (US), Spain. The sample from the Tinto Estuary was immediately

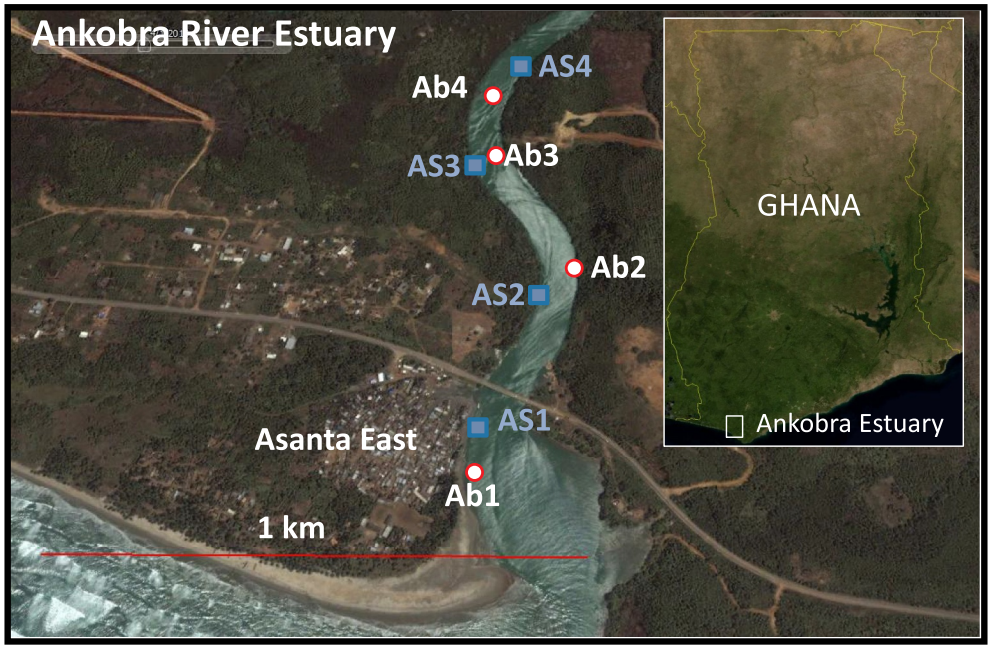

Fig. 2. Sampling sites for surficial sediments in the Ankobra Estuary (Ghana), Ab*i* samples were processed as bulk samples, while AS*i* samples (i = 1,2,3,4) were sieved for estimating their Rosin-Rammler particle-size distributions and for granulometric speciation.

transported to the US laboratory and oven-dried at 80 °C till constant weight.

Particle size distributions have been studied for the Tinto sediment and for four samples distributed along the Ankobra Estuary. Oven-dried samples were gently disaggregated using an agate mortar and then passed through a sieving column with mesh sizes of 2500, 1000, 100, 80, 63, 52, 45, 32 and 25 μm (dry sieved without removing organic matter). The cumulative percentages (given as a fraction) at each diameter level, $y(x)$, were then fitted by a Rosin-Rammler particle-size distribution.

It is worth noting that standard procedures for grain size analysis usually involve small amount of sample and may include gentle ultrasonic and/or the use of some dispersing agents such as metaphosphate (e.g. Gammon et al., 2016). Other methodologies involve pretreatments with HCl (Sun et al., 2018). This is unpractical for granulometric speciation due to the large amount of sample to be processed, and because dispersing agents and/or acids may release a fraction of the studied radionuclides. On the other hand, high resolution grain-size analysis (e.g. using laser diffraction techniques) often show multimodal spectra which can be interpreted as the superposition of several log-normal distributions (Gammon et al., 2016). Nevertheless, the Rosin-Rammler approach seems reasonable enough for data on grain size distributions obtained from the sieving method.

Results could be mediated by poor mechanical disaggregation and low sieving yields. In this work both processes were repeated several times for the > 100 μm fraction till negligible changes in the final masses of different sizes were observed. Although it cannot be absolutely discarded that some small particles could be retained in meshes of larger sizes, those passing the mesh necessarily have smaller diameters. Thus, the activity concentration in the smallest grain-size class provides the estimation of the maximum achievable $F(x_c)$ ratio, when compared with the activity concentration of the bulk sample.

For the Tinto sediment, subsamples from all the grain sizes classes were homogenized and sealed in pre-defined vials (see Table S1 in electronic supplementary material, ESM) to prevent escape of ^{222}Rn, and stored for at least 21 days to establish secular equilibrium among ^{226}Ra, ^{214}Bi and ^{214}Pb. An original composite (non-sieved) aliquot was homogenized and sealed in Petri geometry for standard gamma spectrometry analysis. The same procedure was applied for the four non-sieved samples from the Ankobra Estuary, while for the four sieved samples only the smallest grain-size class was submitted for gamma measurements.

Organic matter content was determined by the Loss-On-Ignition (LOI) method. Prior to ignition, sediment samples and empty ceramic crucibles were preconditioned by oven-drying at 105 °C overnight. Ignition of ~2 g of sample material was undertaken in a muffle furnace at 440 °C for 3.5 h.

2.4. Gamma spectrometry analysis

Samples were measured in an extended range Germanium coaxial detector (XtRa) HPGe of 42.1% relative efficiency with 1.95 keV FWHM for ^{60}Co 1332 keV emission and 1.03 keV FWHM for ^{57}Co 0.122 keV emission. Passive shielding is composed of 10 cm lead (65 ± 3 Bq/kg of ^{210}Pb) internally lined with a 5 mm electrolytic copper layer. Calibration processes in energy (range 46.5–2615 keV) and resolution were performed with point sources while efficiency assessment was carried out according to the different cylindrical geometries employed during this work (see Table S1 in ESM). Three different sizes of Petri dishes (namely, 5.10 ± 0.02 mL, 8.65 ± 0.13 mL and 76.0 ± 0.5 mL) were used according to the existing amount of sample. Each Petri dish was filled without void volumes to avoid systematic errors due to radon accumulation at the upmost empty layer (Mauring and Gäfvert, 2013).

For low energy emissions (mainly ^{210}Pb and ^{234}Th), self-absorption corrections were applied according to Mantero et al. (2013). The sealed samples were counted for about 48 h assessing the MDA values (Currie, 1968; Hartwell, 1975) shown in Table S1 (in ESM) for the different radionuclides. The matrices used to prepare the experimental efficiency setup were IAEA-RGU-1 (Uranium ore with secular equilibrium in ^{238}U series) and IAEA-RGTh-1 (Thorium ore with secular equilibrium in ^{232}Th series) reference materials.

Regarding ^{238}U series radionuclides, ^{210}Pb was determined from its 46.5 KeV gamma emission, ^{234}Th from its 63.3 peak (crosschecked with 92.3 KeV peaks). Activity concentrations of ^{226}Ra were estimated through its progeny radionuclides (^{214}Bi and ^{214}Pb), reported as the averaged values for their emissions of 609.3 and 1764 keV for ^{214}Bi, and 295 and 351.9 keV for ^{214}Pb. Concerning radionuclides from the ^{232}Th series, ^{228}Ra was estimated through ^{228}Ac (assessed as the

average values from its 338 and 911 keV emissions), while ^{228}Th was evaluated as an average of ^{212}Pb (from its 238.6 KeV peak), ^{212}Bi (at 727.3 keV) and ^{208}Tl (583.2 and 2614.5 keV). Finally ^{40}K was measured via 1460.8 keV, and the anthropogenic ^{137}Cs by using its 661.3 keV gamma line. For 2-days measurements counting uncertainties ranged from 9% to 40%, and from 3% to 40% for ^{137}Cs and NORM radionuclides respectively (with the lowest values being associated to the 75 mL geometry and the highest values to the 5 mL geometry).

Quality Control checks were performed through routine participation in National (Spanish Nuclear Safety Council, CSN) and International (IA EA and European Commission at JRC) Proficiency Tests (IA EA ,2018). A brief summary of the last two participations where soil matrices were involved is presented in Table S2 in ESM. These Quality Controls served for identifying eventual weaknesses in the methodology and for applying the necessary improvements.

3. Results and discussion

3.1. Rosin-Rammler distributions

The measured cumulative percentages of mass (given as a fraction) at each diameter level for the Tinto and Ankobra sediment samples are presented in Fig. 3, along with the fitted R-R particle size distributions. The fitted parameter values are reported in Table 1, along with the estimated median and modal diameters. The Tinto sediment is the coarsest sample, with a mean diameter of ~114 μm. In the Ankobra Estuary, the two sediments sampled upstream showed higher mean and modal diameter values.

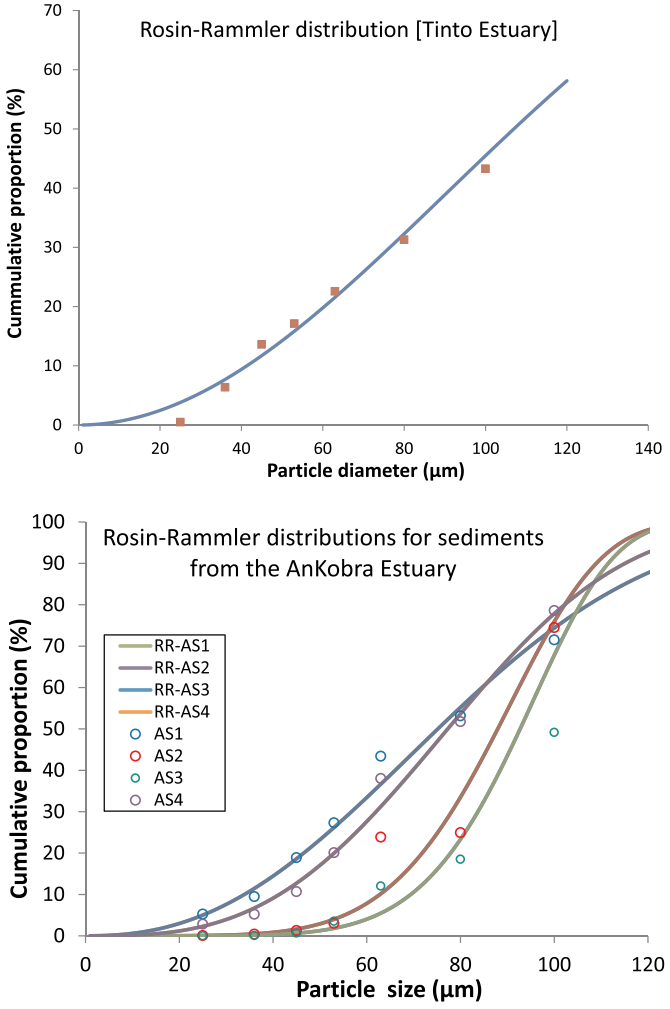

Fig. 3. Cumulative percentages at each diameter level and the fitted Rosin-Rammler particle-size distributions for the sediment samples from the Tinto Estuary (Spain) –panel 1, and the AS*i* samples of the Ankobra Estuary (see Fig. 2) – panel 2. The fitting parameters are reported in Table 1.

Table 1
Parameter values for the Rosin-Rammler particle-size distribution (n and x_0 in Eq. (1)) along with modal and mean values of particles diameter (ϕ) for sediment samples from the Tinto and Ankobra estuaries.

Sample	n	x_0 (μm)	Pearson's r	Mean ϕ (μm)	Modal ϕ (μm)
Tinto Estuary	1.982	128.7	0.986	113.7	90.3
Ankobra AS1	3.108	63.7	0.993	57.0	56.2
Ankobra AS2	1.859	74.9	0.987	66.4	49.5
Ankobra AS3	6.501	98.1	0.967	91.4	95.6
Ankobra AS4	3.013	87.3	0.991	77.9	76.3

Parameters n and x_0 after a least squares fit to the empirical cumulative percentages shown in Fig. 3, with the reported Pearson's r. See Fig. 2 for the sample codes in the Ankobra Estuary.

The obtained R-R distributions allow estimating the minimum amount of dry bulk sediment sample to be processed for getting enough amount of mass of certain grain-size class for a standardized counting geometry. Thus, for the Tinto Estuary, from Eq. (1) and the parameter values of Table 1, $y(25) = 0.038$; so it was necessary to process about 200 g of dry bulk sediment to get enough mass of the < 25 μm grain-size class to fill the smallest counting geometry, P 5 mL. This approach may be useful in exploratory field studies preceding the main sampling campaign, since information obtained may contribute for making decisions on the coring diameter, core sectioning resolution, etc.

In radiometric dating, the available dry bulk mass for each sediment slice is given by the diameter of the coring device, the selected resolution (thickness) and the bulk density (which usually increases downcore). In these cases the R-R distributions allow selecting the cutting diameter for defining a homogenous grain-size class for the whole core length with enough mass for a feasible counting geometry. The set of R-R distributions for the Ankobra sediments (Table 1) can serve for illustrating this point. In the hypothetical case of that about 5 g of sample were needed for a given counting geometry, and the available masses of bulk samples were over 100 g, the cutting diameter must satisfy that $y(x_c) > 0.05$. From Table 1 and panel 2 in Fig. 3, the worst case is for AS3. Solving for x_c from Eq. (1) and parameters from AS3, the cutting diameter is 62 μm.

In practice, for the Ankobra sediment samples, with an initial amount of bulk dry mass of 150 g the $x < 25$ μm fraction was measurable in P 9 mL geometry (a Petri dish of 33 mm diameter) for AS1 and AS4 samples. For AS2 and AS3 it was only possible measuring the $x < 45$ μm fraction in P 5 mL geometry (a Petri dish of 9.8 mm diameter).

3.2. LOI and radionuclide activity concentrations

The measured activity concentrations of the target radionuclides (^{40}K, ^{137}Cs, ^{210}Pb, ^{226}Ra, ^{228}Ra, ^{228}Th and ^{234}Th) in the different grain-size classes of the Tinto sediment are reported in Table 2. Table 3 reports the results for the composite (non-sieved) and the smallest grain-size classes in the sieved sediment samples from the Ankobra Estuary. The above tables also report the organic matter content in all the measured samples, given as the LOI_{440} percentage.

Sediments from the Tinto Estuary show strong disequilibria in the radioisotopes from the ^{238}U decay chain. In fact, the ^{234}Th (^{238}U)/^{226}Ra ratio is of 2.75 ± 0.13 in the non-sieved sample, being far from the secular equilibrium. Despite the large involved uncertainties, ^{234}Th activity concentrations show a pattern of increase with decreasing particle diameter (Table 2). It is known that effluents from the acid mining drainage occurring upstream carry high concentrations of ^{238}U (Villa et al., 2011; Hierro et al., 2013) and its decay product, ^{234}Th,

Table 2
LOI and specific activities[a] of radionuclides in different grain-size classes of sediments from the Tinto Estuary.

Diameter, x (μm)	Geom.	LOI (%)	^{40}K	^{137}Cs	^{210}Pb	^{226}Ra	^{228}Ra	^{228}Th	^{234}Th
			(Bq/kg)						
$x < 25$	P 5 mL	8.08	440 ± 370	5.8 ± 1.6	128 ± 50	60 ± 23	39 ± 16	21 ± 18	170 ± 50
$25 \leq x < 36$	P 9 mL	9.51	433 ± 130	5.1 ± 0.4	115 ± 20	57 ± 7	26 ± 8	30 ± 9	126 ± 21
$36 \leq x < 45$	P 9 mL	9.03	570 ± 130	3.6 ± 2.9	149 ± 18	60 ± 4	41 ± 7	39 ± 10	141 ± 19
$45 \leq x < 53$	P 9 mL	9.08	400 ± 100	4.1 ± 1.4	101 ± 14	37 ± 8	32 ± 7	29 ± 4	137 ± 15
$53 \leq x < 63$	P 9 mL	8.84	440 ± 110	5.5 ± 0.4	143 ± 16	49 ± 4	36 ± 3	53 ± 5	162 ± 17
$63 \leq x < 80$	P 9 mL	8.46	440 ± 90	2.7 ± 1.4	124 ± 13	52 ± 2	33 ± 6	31 ± 4	145 ± 15
$80 \leq x < 100$	P 9 mL	8.68	370 ± 100	3.6 ± 1.1	141 ± 15	49 ± 8	24 ± 10	38 ± 10	112 ± 16
$100 \leq x < 1000$	P 9 mL	7.81	410 ± 100	3.6 ± 2.0	107 ± 13	44 ± 8	23 ± 7	31 ± 7	124 ± 15
$x < 2500$	P 75 mL	7.38	448 ± 26	3.1 ± 0.3	119 ± 4	46.4 ± 1.1	28 ± 4	32.5 ± 1.3	128 ± 5
Est. $x < 1000$	–	7.31	370 ± 60	3.3 ± 0.5	105 ± 8	42 ± 4	24 ± 3	30 ± 3	113 ± 7

Geometries: P 5 mL P 9mL and P 75 mL are Petri dishes of 19.6 mm 32.8 mm and 86.6 mm of internal diameter, respectively (see Table S1 in ESM).
$x < 2500$ is the composite (non-sieved) sediment sample. and "Est. $x < 1000$" is the value calculated from the specific activity concentration and the relative abundance of each grain-size class (in Fig. 2).
[a] Mean and 1σ counting uncertainties.

shows strong affinity for suspended particulate matter and surficial sediments, what explains the observed enrichment and the congruent particle-size effect.

The ^{226}Ra/^{228}Ra ratio is close to unity in the earth crust, but the value of 1.66 ± 0.24 (non-sieved sediment) found in this work reveals an enrichment in ^{226}Ra, what can be explained by the impacts of the ^{226}Ra-reach phosphogypsum released in the past decades by the phosphate-fertilizer industries (García-Tenorio et al., 2015).

Lead-210 activity concentrations (Table 2) are contributed by their supported (from the *in situ* radioactive decay of ^{226}Ra) and unsupported (^{210}Pb$_{exc}$, from the radioactive decay of ^{222}Rn in the atmosphere) fractions. The value of its activity concentration in the non-sieved sample, 119 ± 4 Bq/kg, compares well with other reported values for surficial sediments in this geographical area (e.g. San Miguel et al., 2004; Abril et al., 2018).

Caesium-137 was measured in the non-sieved sample of sediments from the Tinto Estuary, with a value (3.1 ± 0.3 Bq/kg) which compares well with those reported by San Miguel et al. (2004) for surficial sediments sampled in this estuary. Potasium-40 shows typical values without noticeable particle-size effects (Table 2), likely owing to detrital mineral composition.

Sediments from the Ankobra Estuary (non-sieved samples) show overall lower concentrations for the radioisotopes from the ^{238}U and ^{232} Th decay series. The ^{234}Th (^{238}U)/^{226}Ra ratio is 1.03 ± 0.19 (mean and 1-σ standard deviation), indicative of secular equilibrium. The ^{226}Ra/^{228}Ra ratio is 1.34 ± 0.06, close to the reference value for the earth crust. The same is true for the ^{234}Th/^{228}Th ratio. In addition, ^{210}Pb is found in excess with respect to ^{226}Ra, with values which compares well with those reported by Klubi et al. (2017) for sediment cores from the Pra and Volta estuaries, also in Ghana. ^{137}Cs was under the detection limit in all the samples. ^{40}K was found in concentrations similar to those from the Tinto Estuary, exception of the sample Ab1, with an anomalous low value of 114 ± 9 Bq/kg.

The LOI percentage in the different grain-size classes of sediments from the Tinto Estuary was relatively uniform, within the range from 7.8% to 9.5%, and with slightly lower values associated to the larger grain sizes (Table 2). In the Ankobra Estuary the LOI values were overall lower than in the Tinto (range from 1.4% to 4.8%), with the sieved samples having similar or lower values than their respective paired reference samples, with the exception of AS1. Consequently, the potential effect of granulometry in the organic matter content cannot be distinguished from the spatial variability. The used methodology does not provide information on whether organic matter is present as particle-coatings and/or as fragments of different sizes.

3.3. Grain size effect in ^{137}Cs and ^{210}Pb activity concentrations

Fig. 4 shows the measured ^{137}Cs activity concentrations in the sediment samples from the Tinto Estuary as a function of the central diameter of each grain-size class, along with the concentrations reported by Alonso Hernández et al. (2006) as a function of the mean grain size for surficial sediments from the Cienfuegos Bay (Cuba) –their Table 1. Fig. 4 also plots, for the sake of comparison, the expected decrease of ^{137}Cs activity concentrations with particle diameter given by Eq. (3) with the k value solved from Eq. (4) (with the R-R distribution of Fig. 3) and the measured value of A_b in the non-sieved sample (Table 2).

Although ^{137}Cs activity concentrations for $x < 25$ μm were higher than those for the bulk sample (statistically significant at 95% confidence level), there was an overall lack of correlation between ^{137}Cs concentrations and the mean diameters ($r = -0.46$, $p = 0.25$). Furthermore, the pattern is far from the one expected from concentrations governed by the surface area of the sediment particles and the R-R distribution of Fig. 3 ($\chi^2_\upsilon = 19.8$, far from the target value of 1.0; –see definition and statistical significance in Bevington and Robinson, 2003).

Table 3
LOI and specific activities[a] of radionuclides in sediment samples from the Ankobra Estuary.

Sample	Geom.	LOI (%)	^{40}K	^{137}Cs	^{210}Pb	^{226}Ra	^{228}Ra	^{228}Th	^{234}Th
			(Bq/kg)						
Ab1	P 75 mL	1.40	114 ± 9	< 0.4	20.7 ± 1.3	12.1 ± 0.3	9.6 ± 1.5	10.1 ± 0.5	14.6 ± 3.3
AS1 x < 25 μm	P 9 mL	4.75	380 ± 100	< 6.7	87 ± 14	41.7 ± 1.0	28 ± 11	26 ± 11	20 ± 14
Ab2	P 75 mL	4.50	430 ± 20	< 0.8	53 ± 3	29.3 ± 1.2	21.5 ± 0.6	31 ± 1.1	30.2 ± 2.5
AS2 x < 45 μm	P 5 mL	3.64	350 ± 120	< 10	65 ± 25	29 ± 10	37 ± 20	< 18	50 ± 30
Ab3	P 75 mL	4.80	513 ± 23	< 1.0	63 ± 3	32 ± 3	23 ± 4	34.5 ± 1.2	36 ± 4
AS3 x < 45 μm	P 5 mL	4.80	420 ± 190	< 18	103 ± 35	26 ± 10	< 70	< 30	< 200
Ab4	P 75 mL	4.60	498 ± 22	< 1.0	60 ± 3	31.2 ± 2.3	23 ± 4	28.8 ± 1.1	24 ± 7
AS4 x < 25 μm	P 5 mL	3.27	470 ± 110	< 6.4	76 ± 24	28 ± 14	40 ± 26	24 ± 13	< 110
	P 5 mL	2.59	< 467	< 19	41 ± 36	< 54	< 90	< 38	< 250
AS425 < x < 36 μm									

Geometries: P 5 mL, P 9mL and P 75 mL are Petri dishes of 19.6 mm, 32.8 mm and 86.6 mm of internal diameter, respectively (see Table S1, in ESM).
Ab*i* are composite (non-sieved) sediment samples while AS*i* are subsamples from sieving (see Method's section and Fig. 2 for sample identification).
[a] Mean and 1σ counting uncertainties; for non-detected radionuclides the activities are reported as < AMD; x refers to particles diameter.

To avoid any artefact from the continuous R-R distribution (which provides a poor fit for small diameters – see Fig. 3), the stepped function defined by empirical data (the points in Fig. 3 with the diameter intervals given in Table 2) can be alternatively used for estimating ^{137}Cs concentrations in the different grain-size classes. This leads to a value of 27 Bq/kg for $x < 25$ μm, consistently higher than the value estimated from the continuous R-R distribution (Fig. 4). For this function $\chi^2_\upsilon = 68$.

The organic matter (LOI in Table 2) did not play any effect on the ^{137}Cs concentration, as inferred from the lack of statistical correlation between both variables ($r = 0.23$; $p = 0.58$).

Despite the poor counting statistics, in particular in the small diameter fractions, the small grain-size particles show lower concentrations than expected from our theoretical estimations (Eqs. (3) and (4) in Fig. 4), what can be explained by the fact that natural conditions are far from the ideal ones occurring in spiked aqueous suspensions. The measured activity concentration in these grain-size fractions is the composite result of many different histories of varying contact times among particles and the aqueous phase with an also varying range of concentrations of dissolved radionuclides. Thus, some of the particles may have low or null activity concentrations because of their peculiar environmental history. On the other hand, the largest grain size shows a concentration higher than expected, which can be at least partially explained by a poor sieving yield, despite the efforts applied in the methodology (Section 2). Nevertheless, it is worth noting that particle coating and aggregation (both increasing the mean diameter) also occur in natural systems. Additionally non-spherical shapes also contribute to larger specific surface area (SSA). Surficial sediments also can uptake dissolved fallout radionuclides from the overlaying water column, but the process is governed by physical diffusion and for the fraction of the particles surface which is actually accessible to the pore-water, instead of their total SSA (Barros et al., 2004).

The representative history of the particles of different sizes is expected to vary with time. The freshly deposited ^{137}Cs around the 1963 peak in atmospheric fallout is expected to have been present mostly in dissolved form in the water column, from where it would have been uptaken by particulate matter according to their SSA, and by surficial sediments. Contrarily, in recent times most of the ^{137}Cs reaches the sediment already bound to particulate matter, according to their provenance and environmental histories. These histories are also expected to be different from site to site.

Data from Cienfuegos Bay are not directly comparable since they refer to mean grain-sizes in the whole sample. Nevertheless, they are congruent with present results, and they reveal noticeable particle-size effects for very small particles diameters only. But in practice, and as above commented, the smallest useful fraction for granulometric speciation and gamma measurements in the scope of radiometric dating is limited by the corer diameter, depth resolution, bulk density and the particle size distribution itself. Thus, in the Ankobra sediments, despite the efforts for selecting the smallest manageable grain-size fraction, ^{137}Cs was below the detection limit in all the cases.

Fig. 5 shows the measured activity concentrations of ^{210}Pb and ^{226}Ra in the sediment samples from the Tinto Estuary as a function of the central diameter of each grain-size class. The involved analytical uncertainties do not allow identifying any clear pattern of variation with particle sizes. Properly, such a pattern of variation was expected for the excess ^{210}Pb, which is attached to the particles surface. Nevertheless, this was not the case for the present dataset (Fig. 5; $r = -0.26$, $p = 0.53$). There was also a lack of correlation between $^{210}Pb_{exc}$ and LOI ($r = 0.08$, $p = 0.85$).

For the sake of comparison Fig. 5 also plots the results reported by Aalto and Nittrouer (2012) for floodplain sediments, with ^{210}Pb measured by α-spectrometry after total acid digestion of the samples. These authors were able to capture a general trend of increasing in the total ^{210}Pb activity concentrations with decreasing particles sizes. This pattern is also observed with statistical significance in some of the samples

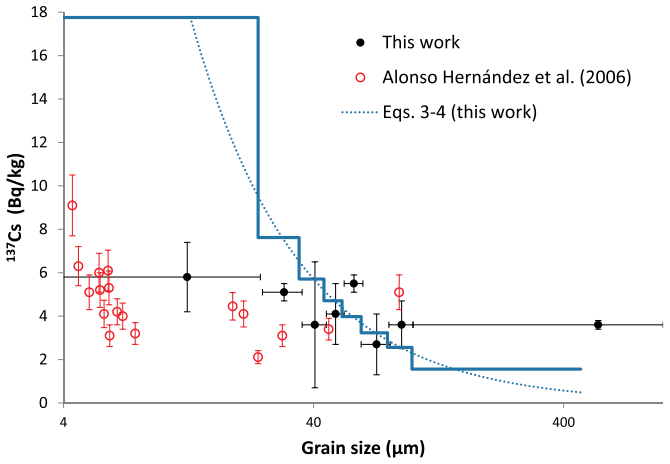

Fig. 4. ^{137}Cs activity concentrations in the sediment samples from the Tinto Estuary as a function of the central diameter of each grain-size class. Vertical bars are 1-σ analytical uncertainties, while horizontal bars define the grain-size interval of each sample. For the sake of comparison, the figure also plots data reported by Alonso Hernández et al. (2006) as a function of the mean grain size for surficial sediments from the Cienfuegos Bay (Cuba) –their Table 1. The stepped and dotted lines plot the activity concentration estimated by Eqs. (3) and (4) and the Rosin-Rammler particle size distribution for this sediment (Fig. 3, panel 1), with $\rho = 2.5\ g{\cdot}cm^{-3}$ and k solved from Eq. (4) by imposing as A_b the measured value of 3.1 Bq/kg in the non-sieved sample (Table 2). The stepped line gives the theoretically estimated values for the same grain-size intervals than the experimental values.

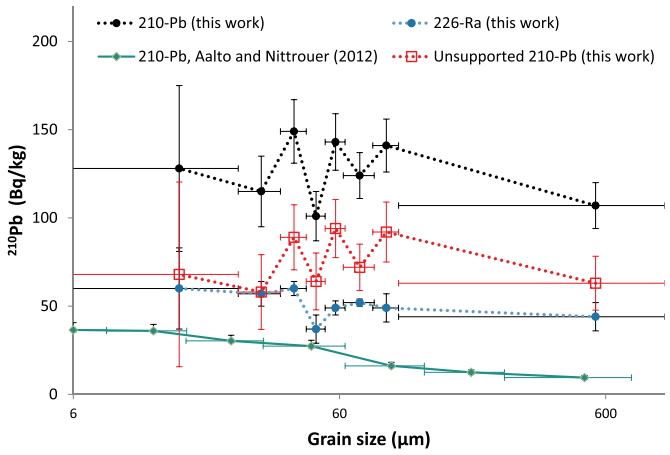

Fig. 5. Activity concentrations of ^{210}Pb, ^{226}Ra, and ^{210}Pb$_{exc}$ in the sediment samples from the Tinto Estuary as a function of the central diameter of each grain-size class. Vertical bars are 1-σ analytical uncertainties, while horizontal bars define the grain-size interval of each sample. For the sake of comparison Fig. 5 also plots the results reported by Aalto and Nittrouer (2012) for flood-plain sediments, with ^{210}Pb measured by α-spectrometry after total acid digestion of the samples.

of the Ankobra Estuary, when compared with their respective non-sieved pairs (Table 3).

3.4. On the use of granulometric speciation for assisting radiometric dating

Coming back to Eq. (5), present results show that the assumptions involved in the theoretical estimation of the factor $F(x_c)$ do not necessarily hold for environmental conditions. With the manageable amount of mass used in this work, the maximum empirical value for $F(x_c)$ was 1.9 ± 0.6 for ^{137}Cs in the $x < 25$ μm grain-size fraction (Table 2), while it was 0.9 ± 0.7 for ^{210}Pb$_{exc}$. But the ratio of masses used in geometries P 9 mL and P 75 mL was about 1/8, with little improvement in the counting efficiency (a factor 1.5 for ^{137}Cs and 2.1 for ^{210}Pb; see Table S1 in ESM). Thus, the overall balance gives F_N values below 1.

In our experimental settings, the poor counting statistics for ^{137}Cs and ^{210}Pb measurements, in particular in the small diameter fractions, might mask a possible trend of increasing activity concentrations with decreasing particle diameters (Table 2 and Figs. 4 and 5). Nevertheless, from Fig. 4 it is also clear that such a trend would be considerably weaker than the one expected from our theoretical estimations (Eqs. (3) and (4)). As it was commented previously, the empirical estimation of $F(x_c)$ is not mediated by any sieving artefacts. Its maximum achievable value is limited by the R-R particle size distribution of the sediments and for the minimum amount of mass manageable for gamma spectrometry. But the major result from this work is that under actual environmental conditions this ratio does not necessarily follow the expected increase with SSA, and this failure cannot be compensated in our study by any strategy for increasing the mass of the bulk sample or the counting efficiency. This provides caution on granulometric speciation as a tool of general use for improving the quantification of fallout ^{137}Cs for assisting the dating of recent sediments from the south hemisphere.

Table S1 (in ESM) shows that the major contributor to the improvement of MDA values is the mass of the sample. Thus, instead of granulometric speciation, the above commented strategies for increasing the available amount of mass of bulk sample (e.g., increasing the corer diameter, twin cores, thicker slicing resolution …) could be used in combination with geometries allowing for large masses along with good counting efficiencies (such as Marinelli 250 mL).

3.5. On the use of granulometric normalization in radiometric dating

Concerning normalization in ^{210}Pb-based radiochronologies, it is worth noting that it is not necessary for the application of the Constant Rate of Supply (CRS) model. More properly, the CRS model does not work with normalized concentrations. The CF-CS model arises as a particular case of the CRS model; nevertheless, using normalized ^{210}Pb$_{exc}$ values with the CF-CS model is at least justified in cases of incomplete recovery of inventories. On the other hand, normalization is consistent with the fundamentals of the CIC model.

The fundamentals of normalization by particle size rely on distinguishing two grain-size classes separated by the cutting diameter x_c; the fine-size has a mass fraction $y(x_c)$ and an average activity concentration A_f, while the large-size fraction has a mass fraction 1- $y(x_c)$ and a mean activity concentration A_l. The experimentally measured value is the activity concentration in the bulk sample, A_b, is related with the above magnitudes in the way: $A_b = y(x_c)\ A_f + (1\text{-}\ y(x_c))\ A_l$.

For granulometric normalization it is assumed that A_l is close to zero in all the sediment slices. Under this assumption $A_f \approx A_b/y(x_c)$. As this applies for each individual sediment slice, the normalized magnitude for the sediment slice of index i, is defined as follow:

$$A_{N,\,i} = A_{b,\,i}\frac{\bar{y}\,(x_c)}{y_i(x_c)} \tag{7}$$

where $\bar{y}\,(x_c)$ is the averaged value over the whole measured core length.

In most of the applications the cutting diameter is set at 63 μm (normalization to mud content). Nevertheless, present results reveal that the assumption that the sand fraction ($x > 63$ μm) of a sediment slice has a negligible ^{210}Pb$_{exc}$ content when compared with the complementary grain-size class, is not of general applicability, posing then serious constrains in the use of mud-normalized concentrations. The present work did not split the region below 25 μm into smaller grain-size classes. Results from Aalto and Nittrouer (2012), Ontiveros-Cuadras et al. (2012), and Sun et al. (2018), suggest the possibility of using the clay fraction (< 4 μm) for normalization in ^{210}Pb-based radiometric dating models.

4. Conclusions

The present work has reviewed the fundamentals and the feasibility of the practical use of granulometric speciation in the scope of gamma spectrometry for assisting in the radiometric dating of recent sediments. Major conclusions are:

i) Assuming that activity concentrations are proportional to the surface area of the sediment particles, measuring a small grain-size fraction of the sample, along with strategies for maximizing the available mass of bulk sediment and the counting efficiency, could improve the number of counts in the photopeak by a factor F_N, substantially higher than the unity when gamma-ray spectrometry is performed.

ii) Under our experimental settings, the above situation does not hold for the two studied sedimentary environments (the Tinto Estuary, Spain, and the Ankobra Estuary, Ghana). Unlike under ideal experimental conditions, the uptake of radionuclides by suspended particulate matter and surficial sediments in real aquatic environments is the composite result of a large variability of chemical-physical conditions and a large diversity of contact times. Consequently, the observed increase in activity concentrations with decreasing particle sizes is only slight or negligible in the studied cases (Figs. 4 and 5).

iii) Present results provide caution on the use of granulometric speciation as a tool of general applicability for improving the detection of ^{137}Cs in recent sediments with low fallout rates.

iv) Present results reveal that the normalization to the mud content in ^{210}Pb-based radiometric dating models may not be applicable in some cases since in real sedimentary scenarios the mean activity concentration in the sand fraction may not be negligible when compared to that for the mud fraction. Decision on normalization should be taken on case by case basis.

Acknowledgments

The authors would like to extend gratitude to the International A tomic Energy A gency (IA EA)for supporting the Regional Project RAF7009 and the fellowship GHA -16025.

References

Aalto, R., Nittrouer, C.A., 2012. ^{210}Pb geochronology of flood events in large tropical river systems. Phil. Trans. R. Soc. A 370, 2040–2074.

Abril, J.M., Fraga, E., 1996. Some physical and chemical features of the variability of k_d distribution coefficients for radionuclides. J. Environ. Radioact. 30 (3), 253–270. Abril, J.M., 1998a. Basic microscopic theory of the distribution, transfer and uptake kinetics of dissolved radionuclides by suspended particulate matter. Part I: theory development. J. Environ. Radioact. 41, 307–324.

Abril, J.M., 1998b. Basic microscopic theory of the distribution, transfer and uptake kinetics of dissolved radionuclides by suspended particulate matter. Part II: Applications. J. Environ. Radioact. 41, 325–342.

Abril, J.M., 2003. A new theoretical treatment of compaction and the advective-diffusive processes in sediments. A reviewed basis for radiometric dating models. J. Paleolimnol. 30, 363–370.

Abril, J.M., 2015. Why would we use the Sediment Isotope Tomography (SIT) model to establish a ^{210}Pb-based chronology in recent-sediment cores? J. Environ. Radioact. 143, 40–46.

Abril, J.M., San Miguel, E.G., Ruiz-Cánovas, C., Casas-Ruiz, M., Bolívar, J.P., 2018. From floodplain to aquatic sediments: radiogeochronological fingerprints in a sediment core from the mining impacted Sancho Reservoir (SW Spain). Sci. Total Environ. 631–632, 866–878. https://doi.org/10.1016/j.scitotenv.2018.03.114.

Alonso-Hernández, C.M., Diaz-Asencio, M., Muñoz-Caravaca, A., Delfanti, R., Papucci, C., Ferretti, O., Crovato, C., 2006. Recent changes in sedimentation regime in Cienfuegos Bay, Cuba, as inferred from ^{210}Pb and ^{137}Cs vertical profiles. Cont. Shelf Res. 26, 153–167.

Álvarez-Iglesias, P., Quintana, B., Rubio, B., Pérez-Arlucea, M., 2007. Sedimentation rates and trace metal input history in intertidal sediments from San Simón Bay (Ría de Vigo, NW Spain) derived from ^{210}Pb and ^{137}Cs chronology. J. Environ. Radioact. 98, 229–250.

Appleby, P.G., 2001. Chronostratigraphic techniques in recent sediments. In: Last, W.L., Smol, J.P. (Eds.), Tracking Environmental Change Using Lake Sediments. Basin Analysis, Coring, and Chronological Techniques. Developments in Paleoenvironmental Research. Kluwer, Dordrecht, pp. 171–203.

Barros, H., Laissaoui, A., Abril, J.,M., 2004. Trends of radionuclide sorption by estuarine sediments. Experimental studies using ^{133}Ba as a tracer. Sci. Total Environ. 319 (1–3), 253–267.

Barros, H., Abril, J.M., 2005. Constraints in the construction and/or selection of kinetic box models for the uptake of radionuclides and heavy metals by suspended particulate matter. Ecol. Model. 185 (2–4), 371–385.

Bevington, P.A., Robinson, D.K., 2003. In: Data Reduction and Error Analysis for the Physical Sciences, third ed. McGraw-Hill, New York.

Carroll, J., Lerche, I., 2003. Sedimentary Processes: Quantification Using Radionuclides. Elsevier, Oxford.

Cundy, A.B., Croudace, I.W., 1996. Sediment accretion and recent sea-level rise in the solent, southern england: inferences from radiometric and geochemical studies. Estuar. Coast Shelf Sci. 43, 449–467.

Currie, L.A., 1968. Limits for qualitative detection and quantitative determination. Application to radiochemistry. Anal. Chem. 40, 586–593.

El-Mrabet, R., Abril, J.M., Manjón, G., García-Tenorio, R., 2001. Experimental and modelling study of Plutonium uptake by suspended matter in aquatic environments from southern Spain. Water Res. 35 (17), 4184–4190.

Gammon, P.R., Neville, L.A., Patterson, R.T., Savard, M., Swindles, G.T., 2016. A log-normal spectral analysis of inorganic grain-size distributions from a Canadian boreal lake core: towards refining depositional process proxy data from high latitude lakes. Sedimentology 64 (3), 609–630 64.

García-Tenorio, R., Bolívar, J.P., Gázquez, M., Mantero, J., 2015. Management of by-products generated by NORM industries: towards their valorization and minimization of their environmental radiological impact. J. Radioanal. Nucl. Chem. 306 (3), 641–648.

Guerrero-Márquez, J.L., Mosqueda-Peña, F., Mantero, J., Manjón, G., García-Tenorio, R., Bolívar, J.P., 2017. Occupational, public and environmental radiological impact caused by the Phosphoric Acid industry; the case of Huelva (Spain). In: Phosphoric Acid Industry - Trends and Technologies. Intech, pp. 1–20. https://doi.org/10.5772/intechopen.68567. 2017.

Hancock, G.J., Leslie, C., Everett, S.E., Tims, S.G., Brunskill, G.J., Haese, R., 2011. Plutonium as a chronomarker in Australian and New Zealand sediments: a comparison with ^{137}Cs. J. Environ. Radioact. 102, 919–929.

Hartwell, J.K., June 1975. ARH-SA-215. Atlantic Richfield Handford Company. s.

Hierro, A., Bolivar, J.P., Vaca, F., Borrego, J., 2012. Behaviour of natural radionuclides in surficial sediments from an estuary impacted by acid mine discharge and industrial effluents in Southwest Spain. J. Environ. Radioact. 110, 13–23.

Hierro, A., Martín, J.E., Olías, M., Vaca, F., Bolívar, J.P., 2013. Uranium behaviour in an estuary polluted by mining and industrial effluents: the Ría of Huelva (SW of Spain). Water Res. 47, 6269–6279.

IAEA, 2018. IAEA Website for Proficiency Tests: https://nucleus.iaea.org/rpst/referenceproducts/Proficiency_Tests/index.htm Last access January 2019.

Kim, G., Hussain, N., Church, T.M., Carey, W.L., 1997. The fallout isotope ^{207}Bi in a Delaware salt marsh: a comparison with ^{210}Pb and ^{137}Cs as a geochronological tool. Sci. Total Environ. 196, 31–41.

Klubi, E., Abril, J.M., Nyarko, E., Laissaoui, A., Benmansour, M., 2017. Radioecological assessment and radiometric dating of sediment cores from dynamic sedimentary systems of Pra and Volta estuaries (Ghana) along the Equatorial Atlantic. J. Environ. Radioact. 178–179, 116–126.

Klubi, E., Abril Hernández, J.M., Nyarko, E., Delgado, A., 2018. Impact of gold-mining activity on trace elements enrichment in the West African estuaries: the case of Pra and Ankobra rivers with the Volta estuary (Ghana) as the reference. J. Geochem. Explor. 190, 229–244.

Laissaoui, A., Abril, J.M., 1999. A theoretical technique to predict the distribution of radionuclides bound to particles in surface sediments. J. Environ. Radioact. 44, 71–84.

Mabit, L., Benmansour, M., Abril, J.M., Walling, D.E., Meusburger, K., Iurian, A.R., Bernard, C., Tarjan, S., Owens, P.N., Blake, W.H., Alewell, C., 2014. Fallout ^{210}Pb as a soil and sediment tracer in catchment sediment budget investigations: a review. Earth Sci. Rev. 138, 335–351.

Mantero, J., Gazquez, M.J., Bolivar, J.P., García-Tenorio, R., Vaca, F., 2013. Radioactive characterization of the main materials involved in the titanium dioxide production process and their environmental radiological impact. J. Environ. Radioact. 120, 26–32.

Mauring, A., Gäfvert, T., 2013. Radon tightness of different sample sealing methods for gamma spectrometric measurements of 226Ra. Appl. Radiat. Isot. 81, 92–95.

Ontiveros-Cuadras, J.F., Ruíz-Fernández, A.C., Sanchez-Cabeza, J.A., Wee-Kwong, L.L., Pérez-Bernal, L.H., 2012. Geochemical fractionation of ^{210}Pb in oxic estuarine sediments of Coatzacoalcos River, Gulf of Mexico. J. Radioanal. Nucl. Chem. 292, 947–956.

Pedersen, J.B.T., Bartholdy, J., Christiansen, C., 2007. ^{137}Cs in the Danish Wadden Sea: contrast between tidal flats and salt marshes. J. Environ. Radioact. 97, 42–56.

Robbins, J.A., 1978. Geochemical and Geophysical applications of radioactive lead isotopes. In: Nriago, J.P. (Ed.), Biochemistry of Lead in the Environment. Elsevier, Amsterdam, pp. 285–393.

Ruiz-Fernández, A.C., Hillaire-Marcel, C., de Vernal, A., Machain-Castillo, M.L., Vásquez, L., Ghaleb, B., Aspiazu-Fabián, J.A., Páez-Osuna, F., 2009. Changes of coastal

sedimentation in the Gulf of Tehuantepec, South Pacific Mexico, over the last 100 years from short-lived radionuclide measurements. Estuar. Coast Shelf Sci. 82 (3), 525–536.

Sánchez-Cabeza, J.A., Ruíz-Fernández, A.C., 2012. ^{210}Pb sediment radiochronology: an integrated formulation and classification of dating models. Geochem. Cosmochim. Acta 82, 183–200.

Sanders, C.J., Smoak, J.M., Waters, M.N., Sanders, L.M., Brandini, N., Patchineelam, S.R., 2012. Organic matter content and particle size modifications in mangrove sediments as responses to sea level rise. Mar. Environ. Res. 77, 150–155. https://doi.org/10.1016/j.marenvres.2012.02.004.

San Miguel, E.G., Bolívar, J.P., García-Tenorio, R., 2004. Vertical distribution of Th-isotope ratios, ^{210}Pb, ^{226}Ra and ^{137}Cs in sediment cores from an estuary affected by anthropogenic releases. Sci. Total Environ. 318, 143–157.

Sun, X., Fan, D., Tian, Y., Zheng, S., 2018. Normalization of excess ^{210}Pb with grain size in the sediment cores from the Yangtze River Estuary and adjacent areas: implications for sedimentary processes. Holocene 28 (4), 545–557.

Van Eaton, A.R., Zimmerman, A.R., Jaeger, J.M., Brenner, M., Kenney, W.F., Schmid, J.R., 2010. A novel application of radionuclides for dating sediment cores from sandy, anthropogenically disturbed estuaries. Mar. Freshw. Res. 61, 1268–1277.

Vesilind, P.A., 1980. The Rosin-Rammler particle size distribution. Resour. Recovery Conserv. 5 (3), 275–277.

Villa, M., Manjón, G., Hurtado, S., Garcia-Tenorio, R., 2011. Uranium pollution in an estuary affected by pyrite acid mining drainage and releases of naturally occurring radioactive materials. Mar. Pollut. Bull. 62 (7), 1521–1529.